Available online at www.sciencedirect.com
ScienceDirect
Journal of Nuclear Materials 366 (2007) 187–197
journal of nuclear materials
www.elsevier.com/locate/jnucmat

Influence of localized deformation on A-286 austenitic stainless steel stress corrosion cracking in PWR primary water

L. Fournier [a,*], M. Savoie [a,b], D. Delafosse [b]

[a] Commissariat à l'Energie Atomique, CEA Saclay DMN/SEMI/LCMI, 91191 Gif-Sur-Yvette, France
[b] Ecole Nationale des Mines de Saint-Etienne, Centre Science des Matériaux et des Structures, UMR CNRS 5146, 158 Cours Fauriel, 42023 Saint-Etienne cedex 02, France

Received 23 October 2006; accepted 4 January 2007

Abstract

The low cycle fatigue (LCF) behaviour of precipitation-strengthened A-286 austenitic stainless steel was first investigated at room temperature under 0.2% plastic strain control. LCF led to hardening for the first 20 cycles and then to significant softening. LCF-induced dislocation microstructure was characterized using both bright and dark-field imaging techniques in transmission electron microscopy. Cycling softening was correlated with the formation of precipitate-free localized deformation bands. The effect of these precipitate-free localized deformation bands on A-286 stress corrosion cracking (SCC) behaviour in PWR primary water was then examined by means of constant extension rate tensile (CERT) tests at 320 °C and 360 °C. Comparative CERT tests were performed on companion specimens with similar yield stress but pre-fatigued to a few cycles (4–8) or between 125 and 200 cycles. Specimens pre-fatigued to a few cycles with no precipitate-free localized deformation bands exhibited little susceptibility to intergranular SCC (IGSCC). In contrast, the presence of precipitate-free localized deformation bands formed by pre-fatigue to between 125 and 200 cycles strongly promoted IGSCC. The interest of the approach used in this study is to provide insight into the role of localized deformation in irradiation assisted stress corrosion cracking.

1. Introduction

The intergranular cracking of irradiated austenitic stainless steel structural components of nuclear reactor cores is a complex form of material degradation described as irradiation assisted stress corrosion cracking (IASCC). The complexity of IASCC arises from the fact that irradiation has an impact on both the material properties and the environment chemistry. Reviews of state of knowledge of IASCC [1–3] listed water radiolysis, radiation-induced segregation (RIS) at grain boundaries, radiation-induced hardening via the formation of Frank loops, localized deformation, irradiation creep, and transmutation as possible contributors to IASCC in light water reactors. Dissolved hydrogen in PWR primary water completely suppresses water radiolysis preventing detrimental changes in corrosion or redox potentials and therefore SCC susceptibility. While the development of both radiation-induced

* Corresponding author. Tel.: +33 1 69 08 94 20; fax: +33 1 69 08 93 24.
E-mail address: lionel.fournier@hotmail.com (L. Fournier).

0022-3115/$ - see front matter © 2007 Elsevier B.V. All rights reserved.
doi:10.1016/j.jnucmat.2007.01.001

changes in microstructure and microchemistry at grain boundaries is reasonably well understood, the exact influence of these changes on IASCC is unclear. Busby et al. [4] performed post-irradiation annealing tests that preferentially remove dislocation loop damage from proton-irradiated austenitic stainless steels, while leaving RIS largely unchanged, in order to isolate the effect of RIS on IASCC in boiling water reactor normal water chemistry. The authors concluded that both Cr depletion and radiation-induced hardening via the formation of Frank loops are not sufficient to cause IASCC alone. Fukuya et al. [5] also used post-irradiation annealing tests on CW 316L SS neutron-irradiated to 25 dpa to clarify the role of microstructural and microchemical effects on IASCC in simulated PWR primary water. They correlated changes in IASCC behaviour with changes in microstructure and hardening but not with change in RIS. Localized deformation may also play a significant role by inducing stress concentrations at grain boundaries and promoting IG cracking.

Much of the current knowledge on localized deformation in irradiated metals arises from studies on pure metals such as Cu [6,7], Fe [8,9] and Mo [10]. During post-irradiation deformation tests performed on pure metals, mobile dislocations sweep away irradiation defects resulting in the formation of irradiation defect-free channels. Localized deformation in irradiated austenitic stainless steels has received an increasing attention these past years. Irradiated austenitic stainless steels exhibit strain localization both by twinning and by channelling. The occurrence of the two phenomena is influenced by temperature, dose, strain rate and strain. The recent study of Cole et al. [11] showing no strain localization for a 12% CW 316SS irradiated up to 41 dpa and strained at 10^{-3} s^{-1} and 10^{-7} s^{-1} at temperatures between 383 °C and 443 °C suggests that temperature is of the main importance. Overall, twinning is favoured by low dose, low temperature and high strain rate [12–17]. Conversely, channeling is promoted by high dose, high temperature and low strain rate [12–14]. Recently Jiao et al. [18] suggested a possible correlation between IASCC and the degree of localized deformation but could not unambiguously isolate the effect of localized deformation in proton-irradiated stainless steels with various chemical composition and therefore different stacking fault energy (SFE).

In this work, an alternative approach is proposed to determine the specific role of localized deformation on austenitic stainless steel SCC in simulated PWR primary water. Precipitation-strengthened A-286 austenitic stainless steel with a specific ageing heat treatment avoiding grain boundary η phase precipitation was used. Strain localization was obtained by low cycle fatigue (LCF) at fixed plastic strain amplitude at room temperature and characterized by transmission electron microscopy (TEM). A-286 specimens with and without localized deformation bands were strained to failure in a simulated PWR primary water environment. Comparison of the cracking susceptibility between A-286 with and without localized deformation bands shows that strain localization significantly promotes SCC in simulated primary water.

2. Experimental procedure

The chemical composition of the A-286 used in this work is given in Table 1. Grain size was determined after mechanical polishing with wet SiC abrasive paper down to 1 μm roughness and chemical etching at room temperature in a 30 cc HCl, 30 cc HNO_3, 20 cc CH_3COOH and 20 cc H_2O solution for 30 s. An average grain size of 6 μm was measured. All specimens were machined out of a 12.5 mm diameter rod provided by UGITECH. Prior to ageing, all specimens were encapsulated under primary vacuum in quartz tubes, solution annealed at 930 °C for 1 h and water quenched. The effect of ageing heat treatment on the same A-286 precipitation-hardened austenitic stainless steel was studied in a previous work [19] by the same authors, paying particular attention to γ' and η phase precipitation. In the present study, an ageing heat treatment of 50 h at 670 °C was chosen. This ageing heat treatment of 50 h at 670 °C leads to γ' mean diameter, volume fraction and density of 4.6 nm, 0.8% and 1.6×10^{23} m^{-3} respectively, and does not lead to intergranular η phase precipitation that may complicate the interpretation of the results.

Smooth specimens with a 7 mm diameter and a 20 mm gauge length were used for LCF testing. All specimens were mechanically polished with SiC paper down to grit 4000 prior to LCF testing. LCF tests were conducted in air and at room temperature under 0.2% plastic strain control at $R = -1$ and 0.05 Hz, up to 1000 cycles.

Localized deformation bands obtained by LCF were characterized by TEM using a TECNAI FEI transmission electron microscope operating at

Table 1
Chemical composition of A-286 (in wt%)

Fe	Ni	Cr	Ti	Mn	Mo	V	Al	Cu	Si	Nb	Co	C	P	S
Bal.	25	14.1	1.97	1.65	1.18	0.29	0.18	0.14	0.1	0.08	0.08	0.04	0.02	<0.001

300 kV and equipped with a Gatan CCD digital camera. TEM thin foils were prepared using a Tenupol twin jet electropolishing unit with a 70% ethanol, 20% *n*-butyl alcohol and 10% perchloric acid electrolyte at −20 °C and 70 V. Bright field imaging technique was used to determine the mean width of localized deformation bands. Dark field imaging technique using a 5 μm diameter objective aperture and the superlattice reflexion $(1\,0\,0)_{\gamma'}$ of the $\langle 0\,0\,1\rangle$ zone axis was used to image γ' precipitates. Selected area diffraction pattern and dark-field TEM micrograph showing γ' precipitation are displayed in Fig. 1.

As illustrated in Fig. 2(c), smooth tensile test specimens with a 4 mm diameter and a 20 mm gauge length machined out of the 7 mm diameter and 20 mm gauge length LCF tests specimens were used for SCC testing. All specimens were mechanically polished with SiC paper down to grit 4000 and rinsed with ethanol prior to SCC testing. CERT tests were performed at $1.5 \times 10^{-7}\ s^{-1}$ in simulated PWR primary water (1000 ppm of boric acid and 2 ppm of lithium hydroxide) at 320 °C and 360 °C in a 0.88 l austenitic stainless steel static autoclave. All tests were conducted with a 30 cc/kg H_2O dissolved hydrogen concentration controlled with a Pd/Ag probe. Engineering stress–strain curves were post-processed by linearly fitting the elastic part to a Young's modulus of 200 GPa. Analysis of the fracture surface after CERT testing was carried out using a field emission gun (FEG) – scanning electron microscope (SEM). Specimens were ultrasonically cleaned first for 2 h in a 20 cc hydrochloric acid and 80 cc water solution with 2 g hexamethylenetetramine inhibitor and then in acetone for 5 min prior to SEM examination in order to remove the oxide layer formed during CERT testing in high temperature water.

3. Results

3.1. Strain localization by LCF

Typical evolutions of half of the stress amplitude as a function of the number of fatigue cycles at 0.2% plastic strain control, $R = -1$ and 25 °C for A-286 specimens solution annealed (SA) at 930 °C for 1 h, and SA + 50 h aged at 670 °C are displayed in Fig. 3. SA and aged A-286 specimens exhibit totally different LCF behaviour. The SA A-286 specimen work-hardens for the first 50 cycles and then reaches a plateau regime with no further evolution of the flow stress up to 1000 cycles. The aged A-286 specimen work-hardens for the first 20 cycles and then exhibits significant softening up to 1000 cycles. LCF tests results are summarized in Table 2. A softening of 87 MPa was observed after 120 fatigue cycles for A-286 SA + 50 h aged at 670 °C. Some

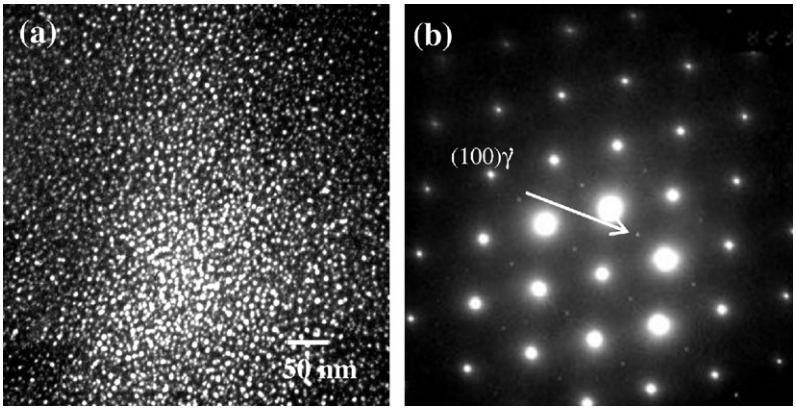

Fig. 1. (a) Dark-field TEM micrograph showing γ' precipitates in the specimen aged 50 h at 670 °C. The associated diffraction pattern is shown in (b). The precipitates were imaged using $(1\,0\,0)_{\gamma'}$ superlattice reflexion (indicated by an arrow) in zone axis $\langle 1\,1\,0\rangle$.

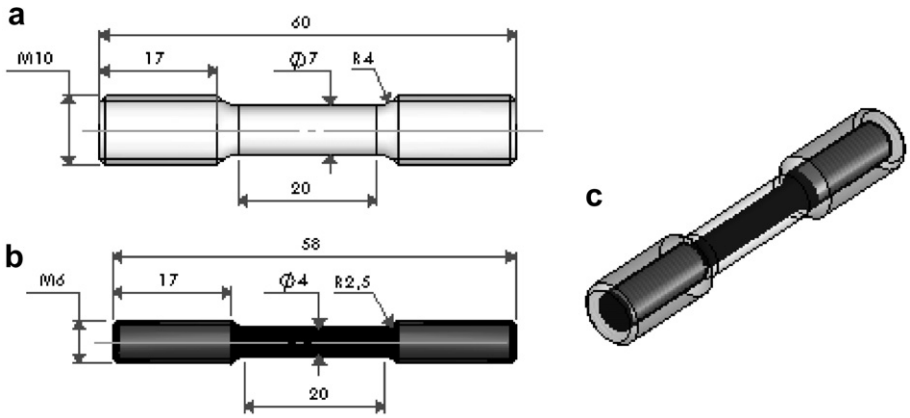

Fig. 2. Schematic representations of (a) the LCF specimens and (b) the tensile test specimens used in this study for SCC testing. (c) Schematic representation of the fabrication of the tensile test specimens by machining from the LCF specimens.

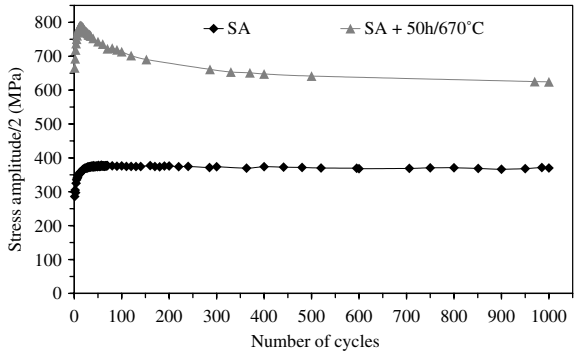

Fig. 3. Evolution of half of the stress amplitude as a function of the number of cycles for SA at 930 °C, and SA + aged 50 h at 670 °C A-286 specimens fatigued at room temperature and $R = -1$ for 0.2% plastic strain control.

crack initiation sites were occasionally observed along the gauge length of aged specimens after 1000 cycles, while no cracks were observed for aged specimens after 200 cycles. A SEM micrograph of the side surface of A-286 aged for 50 h at 670 °C and fatigued to 130 cycles is shown in Fig. 4. Slip traces with a regular spacing are clearly visible and extend through the grains, suggesting that softening is associated with the formation of localized deformation bands.

A typical bright field TEM micrograph of the dislocation microstructure after 120 fatigue cycles at 0.2% plastic strain half-amplitude and room temperature is displayed in Fig. 5. Intense localized deformation bands and diffuse localized deformation bands either lying in a secondary slip system or filling the space between intense bands in the primary slip direction are observed, confirming that LCF softening is correlated with strain localization in bands.

Typical dark-field TEM micrographs using the superlattice reflexion $(1\,0\,0)_{\gamma'}$ of the $\langle 0\,0\,1\rangle$ zone axis to image γ' precipitates are displayed in Fig. 6 for A-286 specimen after 120 fatigue cycles. Localized deformation bands clearly appear to be depleted

Table 2
Results summary of LCF tests performed at room temperature and $R = -1$ for 0.2% plastic strain control on SA at 930 °C, and SA + aged 50 h at 670 °C A-286 specimens

Heat treatment	Maximum $\Delta\sigma/2$ (MPa)	$\Delta\sigma/2$ at 120 cycles (MPa)	Softening at 120 cycles (MPa)
Solution annealed	378	–	–
SA + 50 h/670 °C	789	702	87

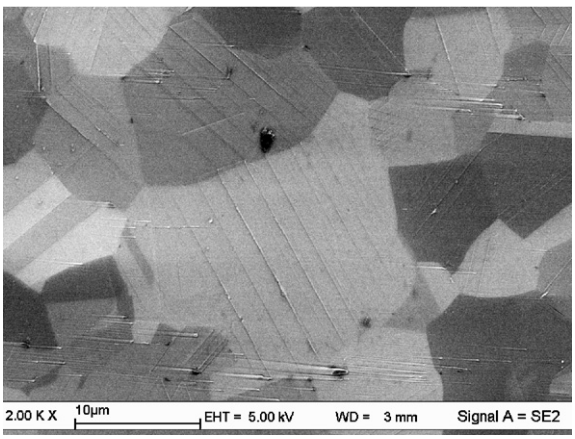

Fig. 4. SEM micrograph of the side surface of a SA + aged 50 h at 670 °C A-286 specimen after 130 cycles of LCF at room temperature and $R = -1$ for 0.2% plastic strain control.

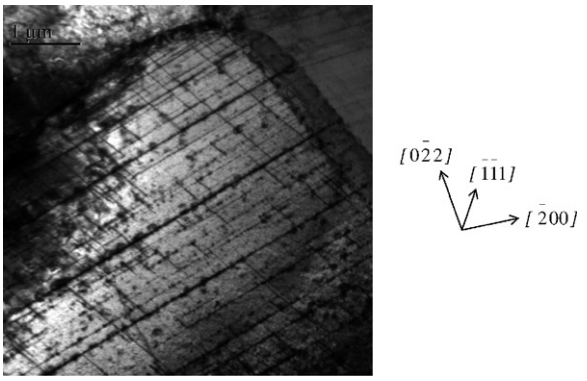

Fig. 5. Bright field TEM micrograph showing localized deformation bands in A-286 specimen after 120 cycles of LCF at room temperature and $R = -1$ for 0.2% plastic strain control. $\langle 0\,0\,1\rangle$ zone axis. Notice the presence of intense localized deformation bands and of less intense bands sometimes on a different slip system.

in γ' precipitates. As it can be seen from Fig. 6, the spacing and thickness of γ'-free bands seem to correspond to the intense slip bands lying in the primary slip system observed in bright field microscopy. It is thus believed that the overall softening is due to these intense slip bands. A statistical analysis of the spatial distribution of these intense slip bands was carried out over 17 grains from four different TEM foils sampled from a specimen after 120 fatigue cycles. Localized deformation bands width and spacing distributions for A-286 after 120 fatigue cycles are displayed in Figs. 7 and 8, respectively. Average localized deformation bands width and spacing of 30 nm and 550 nm were determined respectively.

3.2. Effect of strain localization on SCC

The results of the CERT tests performed in simulated PWR primary water at 320 °C and 360 °C on A-286 specimens with or without localized deformation bands formed by pre-fatigue are summarized in Table 3. The yield stress, ultimate tensile stress, strain-to-failure, percentage of intergranular cracking, and the maximum intergranular crack depth were tabulated for each specimen. It should be noted here that significantly lower yield strengths were measured at 320 °C than at 360 °C. Part of this difference arises from the high temperature sensitivity of the flow stress in the dynamic strain ageing regime. Indeed, DSA was clearly identified and tensile testing showed a 10 MPa lower yield stress at 320 °C than at 360 °C in Ref. [19]. The remainder

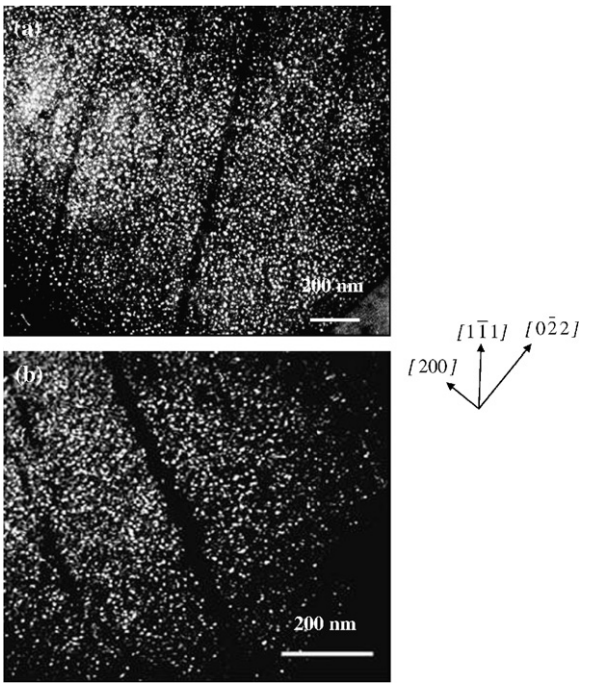

Fig. 6. (a) and (b) Dark field TEM micrographs showing γ' precipitates-free localized deformation bands in A-286 specimen after 120 cycles of LCF at room temperature and $R = -1$ for 0.2% plastic strain control. $\langle 0\,0\,1\rangle$ zone axis.

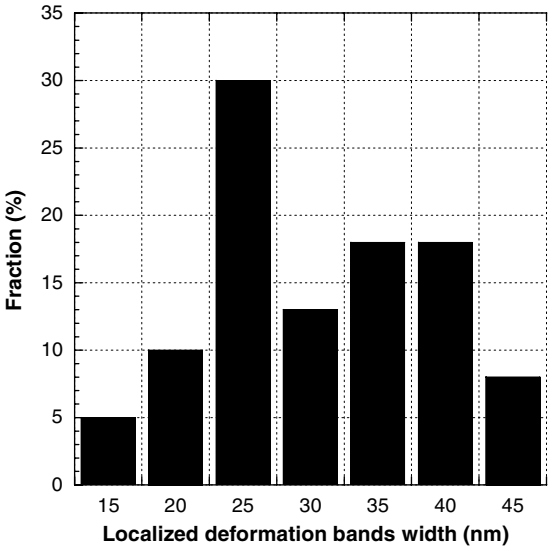

Fig. 7. Localized-deformation bands width distribution for A-286 after 120 cycles of LCF at room temperature and $R = -1$ for 0.2% plastic strain control.

of this difference may be attributed to specimen variability in the LCF behaviour. Stress–strain curves corresponding to CERT tests performed at

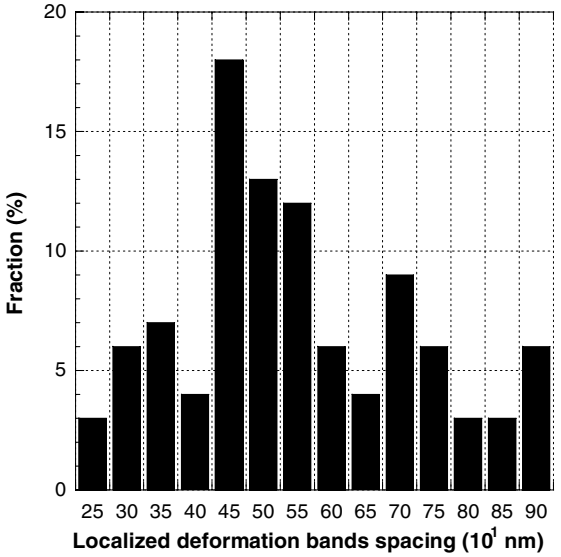

Fig. 8. Localized deformation bands spacing distribution for A-286 after 120 cycles of LCF at room temperature and $R = -1$ for 0.2% plastic strain control.

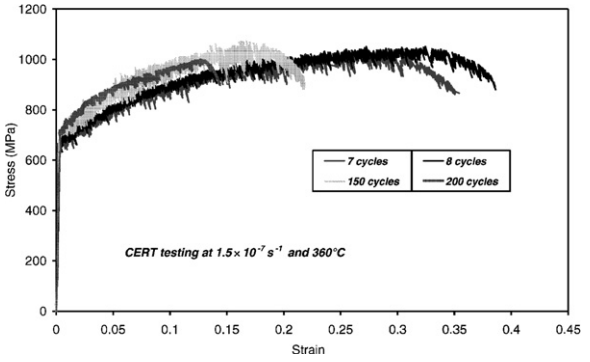

Fig. 9. Stress–strain curves corresponding to CERT tests performed at 1.5×10^{-7} s^{-1} in PWR primary water at 360 °C for A-286 specimens pre-fatigued to 7, 8, 150, and 200 cycles.

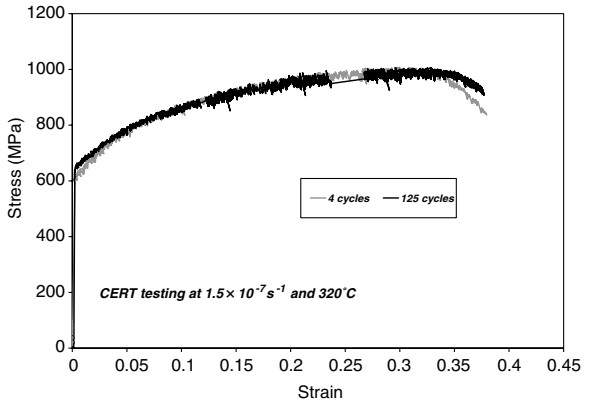

Fig. 10. Stress–strain curves corresponding to CERT tests performed at 1.5×10^{-7} s^{-1} in PWR primary water at 320 °C for A-286 specimens pre-fatigued to 4, and 125 cycles.

1.5×10^{-7} s^{-1} in PWR primary water at 360 °C for A-286 specimens pre-fatigued to 7, 8, 150, and 200 cycles, and at 320 °C for A-286 specimens pre-fatigued to 4, and 125 cycles are displayed in Figs. 9 and 10 respectively. SEM micrographs of the fracture surfaces for an A-286 specimen pre-fatigued to 8 cycles and then strained in simulated primary PWR water at 360 °C, pre-fatigued to 200 cycles and then strained in simulated primary PWR water at 360 °C, and pre-fatigued to 125 cycles and then strained in simulated primary PWR water at 320 °C are displayed in Figs. 11, 12(a) and (b) respectively.

A previous study by the same authors [19] demonstrated a strong correlation between A-286 yield stress and its susceptibility to SCC in PWR primary water. A particular attention was therefore paid in this study to compare specimens with the same yield stress and with or without localized deformation

Table 3
Results summary of CERT tests performed at 1.5×10^{-7} s^{-1} in simulated PWR primary water at 320 °C and 360 °C on pre-fatigued A-286 specimens

Number of pre-fatigue cycles	Test temperature (°C)	Yield stress (MPa)	UTS (MPa)	Strain to failure (%)	% IGC on fracture surface	Maximum crack depth (μm)
4	320	617	1008	38	0	0
125	320	650	1005	37.5	1	256
8	360	683	1046	39	0.4	90
200	360	703	999	14	16	1125
7	360	684	1020	35.4	0.7	160
150	360	703	1060	21.9	5	720

The SCC behaviour of specimens pre-fatigued to 125–200 cycles in order to form localized deformation bands is compared with specimens pre-fatigued to a few cycles (4–8) that do not contain localized deformation bands and have a similar yield stress.

bands. As displayed in Table 3, A-286 specimen pre-fatigued to four cycles exhibit a slightly lower yield stress than the companion specimens tested at 320 °C in PWR primary water due to a stop of the cycling at 0% plastic deformation instead of 0.2%. However, as shown in Fig. 10, the flow stress of the four cycles specimen quickly reaches the flow stress of the 125 cycles specimen and stress–strain curves are almost similar, suggesting no strong effect of the initial difference in yield stress on the final result. For the other companion specimens tested at 360 °C, very similar yield stress were achieved allowing the unambiguous determination of the influence of localized deformation bands on A-286 IGSCC in PWR primary water.

A-286 specimens pre-fatigued to four and 125 cycles and strained in PWR primary water at 320 °C exhibit respectively no and limited IGSCC susceptibility with 1% IG cracking on the fracture surface. A-286 specimens pre-fatigued to 7 and 8 cycles and strained in PWR primary water at 360 °C exhibit limited IGSCC susceptibility with respectively 0.4% and 0.7% IG cracking on the fracture surface, while specimens pre-fatigued to 150 and 200 cycles and strained in PWR primary water at 360 °C exhibit significant IGSCC susceptibility with respectively 5% and 16% IG cracking on the fracture surface. These results obtained for specimens with identical yield stress and with or without localized deformation bands demonstrate the deleterious influence of strain localization on IGSCC. The fact that the existence of localized deformation does not result in a large amount of IGSCC at 320 °C is interpreted in terms of the difficulty to initiate IGSCC at this temperature, as it is shown by the absence of IG cracking for the four cycles specimen at this temperature. This probably stems from the important difference in yield strength between the specimens tested at 320 and 360 °C, although as discussed above the origin of this difference is not fully determined yet. However, the effect of the localised deformation bands remains qualitatively the same: when comparing specimens with the same yield stress, no IG cracking is observed at 320 °C for

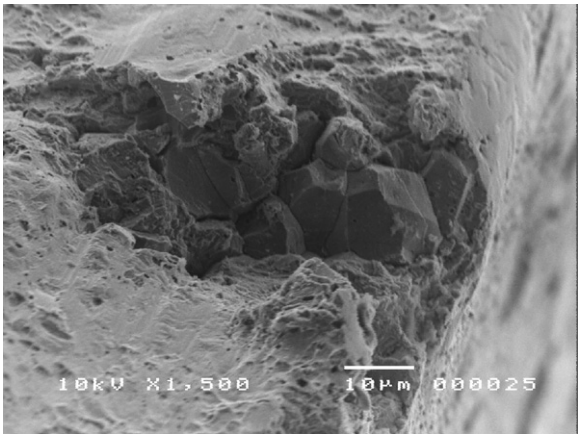

Fig. 11. SEM micrograph of the fracture surface of A-286 specimen pre-fatigued to 8 cycles at room temperature and $R = -1$ for 0.2% plastic strain control and then strained in simulated primary PWR water at $1.5 \times 10^{-7}\,s^{-1}$ and 360 °C showing limited IG crack propagation.

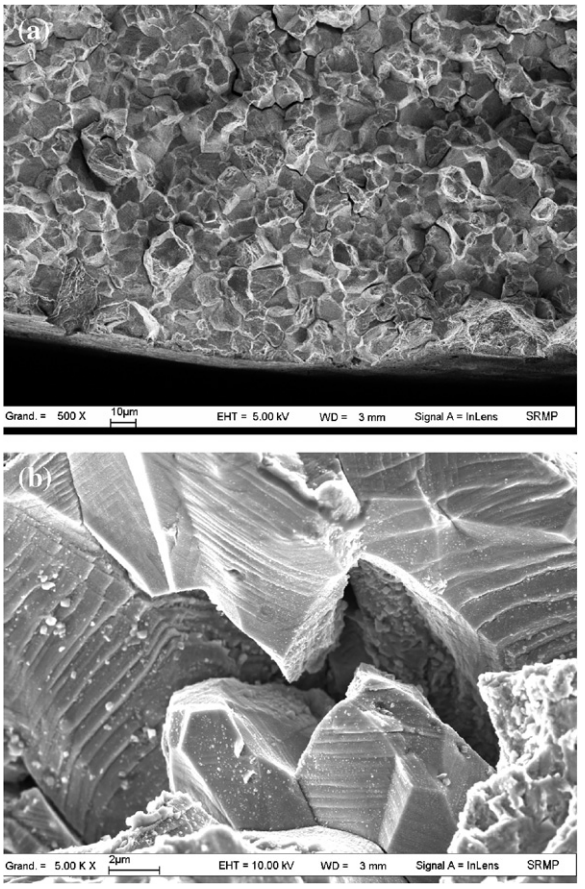

Fig. 12. (a) SEM micrograph of the fracture surface of A-286 specimen pre-fatigued to 200 cycles at room temperature and $R = -1$ for at 0.2% plastic strain control and then strained in simulated primary PWR water at $1.5 \times 10^{-7}\,s^{-1}$ and 360 °C showing extensive IG cracking. (b) High magnification SEM micrograph of the fracture surface of A-286 specimen pre-fatigued to 125 cycles at room temperature and $R = -1$ for 0.2% plastic strain control and then strained in simulated primary PWR water at $1.5 \times 10^{-7}\,s^{-1}$ and 320 °C showing steps on grain boundary facets corresponding to localized deformation bands formed by pre-fatigue.

the four cycles specimen, whereas a limited but significant amount of IG cracking (1%) is obtained after cyclic softening during 125 cycles.

4. Discussion

4.1. Strain localization microstructure

In this study, aged A-286 was clearly shown to exhibit cycling softening associated with the formation of localized deformation bands. Strain localization during cycling loading has been extensively studied in the past. In single phase FCC metals with an intermediate stacking fault energy, slip is confined to persistent slip bands (PSB) during cyclic loading at a given amplitude range [20]. PSB's are characterized by a so-called ladder or wall structure, and the annihilation of edge dislocations in the walls resulting in the production of vacancies and the formation of extrusions on the free surface. Localized deformation bands formed during cycling loading of precipitation-hardened alloys have a more complex structure than classical PSB's [21]. They are also thinner than classical PSB's and are difficult to characterize by TEM. The precise structure of these localized deformation bands formed during cyclic loading on precipitation-hardened alloys is therefore not fully described. In contrast, it is clearly established that strain localization during cycling is due to precipitate shearing. Several authors [22–25] suggested that the movement of a large number of dislocations in the deformation bands causes the precipitates to be gradually sheared off into fragments of sub-critical size, which are thermodynamically unstable and dissolve by themselves. Other authors [26–29] suggested that shearing simply results in precipitate disordering. Sundararaman et al. [30,31] recently attempted to clear this controversy on the dissolution or not of precipitates within the deformation bands for γ' strengthened Nimonic PE16 after LCF at room temperature. These authors performed small angle neutron scattering (SANS) measurements on both fatigued and unfatigued specimens with two different ageing heat treatments. SANS intensity curves as a function of momentum transfer were significantly different for fatigued and unfatigued specimens. A positive difference in the SANS structure function between the fatigued and the unfatigued specimens was observed and correlated with the volume fraction of precipitates which have disappeared during deformation. Relative volume fractions of the initially present precipitates of 8.2% and 6.4% depending on the ageing heat treatment were estimated to have completely disappeared by SANS measurements. Also, no negative difference corresponding to the formation of precipitates with a lower size than the initially present ones was detected in the SANS intensity curves as a function of momentum transfer. Both observations show that gamma prime precipitates have been locally sheared-off and completely dissolved within the localized deformation bands. On the basis of these results, γ' precipitates may be considered completely dissolved in A-286 after 120 cycles at 0.2% plastic strain control and room temperature.

4.2. Effect of localized deformation on SCC

This study was aimed at determining the influence of localized deformation on A-286 SCC susceptibility in PWR primary water, making use of the cyclic softening behaviour of this material associated with the formation of γ' precipitate-free localized deformation bands. Since fatigued A-286 first strain-hardens for a few cycles and then exhibits cyclic softening, it was possible to compare the SCC behaviour of specimens having similar yield stress but with a few fatigue cycles, i.e. specimens with no precipitate-free localized deformation bands; and with numerous fatigue cycles, i.e. specimens with precipitate-free localized deformation bands.

The results described in Section 3.2 clearly demonstrate that the presence of γ' precipitate-free localized deformation bands correlate strongly with the SCC susceptibility of A-286 in PWR primary water. Specimens with a few fatigue cycles that do not contain precipitate-free localized deformation bands exhibit no or little SCC susceptibility while specimens with several tens of fatigue cycles contain precipitate-free localized deformation bands and exhibit significant SCC susceptibility.

The precise mechanism by which localized deformation influences SCC susceptibility is yet to be determined. Assuming that γ' precipitates have been completely dissolved within the localized deformation bands after fatigue, it is believed that at least part of the new dislocations generated during CERT testing will glide along this preferential path and therefore that deformation will continue to be localized within the same bands. This will induce strong pile-ups at grain boundaries possibly favouring local crack initiation. Piled-up dislocations may also

be absorbed by the grain boundary and contribute to grain boundary sliding resulting in the formation of wedge cracks at triple points. TEM analysis of the deformation microstructure at the crack tip may be extremely valuable in the future to determine the precise contribution of localized deformation to IGSCC. Also CERT tests should be regarded as susceptibility tests that do not allow the quantitative evaluation of the specific effect of strain localization on the crack initiation and propagation stages. Other specific SCC initiation and propagation tests on pre-fatigued A-286 are therefore necessary to clarify the impact of localized deformation on initiation and propagation.

4.3. Implication for IASCC

As mentioned in the introduction section, the identification of the mechanism responsible for austenitic stainless steel IASCC is a complex task due to the simultaneous material changes in microstructure, microchemistry and hardening with irradiation. However, Busby and Was [32] identified a possible connection between localized deformation and IASCC. On the basis of this work, Jiao et al. [18] recently examined the effect of stacking fault energy (SFE) and irradiation on deformation mode and IASCC susceptibility using a base 304SS (intermediate SFE), a 304SS + Si (low SFE), and a 304 + Cr + Ni (high SFE) proton-irradiated at 360 °C to 1 and 5 dpa. Localized deformation via channelling was observed in all materials and the degree of localized deformation was found to increase with a decrease in SFE at low dose. Interestingly, the material with the lowest SFE was the most susceptible to IASCC while the materials with the intermediate and high SFE exhibited moderate and no susceptibility to IASCC, respectively. These results support the idea that IASCC is closely related to the degree of deformation localization. However, Si addition in SS was also shown to strongly increase SCC susceptibility in hot water at both oxidizing and reducing corrosion potential [33]. As stated by Li et al. [34], Si addition may affect SCC in various ways including a diminution of the SFE, a decrease in the strength of the oxide, and an increase in the tendency for internal grain boundary oxidation. Data obtained by Raja et al. [35] support a strong detrimental influence of Si addition on passive film stability in high temperature pure water. Si addition is also known to have a significant effect on irradiation-induced microstructure [36]. Understanding the underlying mechanism responsible for the 304SS + Si high susceptibility to IASCC showed by Jiao et al., and isolating the effect of localized deformation on IASCC are therefore not straightforward.

In this context, the approach used in this study may be of particular interest for the understanding of the role of localized deformation on IASCC. Indeed, A-286 γ' mean diameter and density of respectively, 4.6 nm and 1.6×10^{23} m^{-3} used in this study are similar to Frank loops mean diameter and density in neutron-irradiated stainless steels reported by Bruemmer et al. [37] (8 nm and 1.6×10^{23} m^{-3}at 3 dpa for an irradiation at 280 °C) and Pokor et al. [38] (7 nm and 6×10^{22} m^{-3} at 3 dpa for an irradiation at 330 °C). Also, as displayed in Table 4, γ' precipitate-free channels obtained after 120 fatigue cycles with a mean width and spacing of respectively 30 nm and 550 nm, are similar to channels mean width and spacing reported by Farrell et al. [39] in neutron-irradiated 316 SS at 65–100 °C to 0.78 dpa and deformed to 2% strain (26 nm and 622 nm). Finally, as shown in Figs. 12(b), fracture surface of A-286 containing γ' precipitate-free channels and deformed in PWR primary water exhibit steps on grain boundary facets, similar to those in proton-irradiated 304SS strained in BWR environment [40] (Fig. 13(a)), thermally

Table 4
Comparison of localized deformation bands width and spacing for SA + aged 50 h at 670 °C A-286 after LCF at room temperature (This study) with channels width and spacing for 316SS irradiated up to 0.78 dpa and strained up to 32% (From [39])

Material	Strain	Bands/channels width (nm)		Bands/channels spacing (nm)	
		Mean	Standard deviation	Mean	Standard deviation
A-286	120 fatigue cycles	30	7	550	140
316SS 0.17 dpa [39]	6%	10	5	284	200
316SS 0.78 dpa [39]	2%	26	6	622	433
316SS 0.78 dpa [39]	5%	24	5	535	246
316SS 0.78 dpa [39]	32%	19	11	588	306

sensitized 304 SS neutron-irradiated to 1.2×10^{21} n/cm^2 ($E > 1$ MeV) in BWR condition and fractured in inert gas at 290 °C [41] (Fig. 13(b)), and 304 SS neutron-irradiated to 30 dpa at 300 °C and strained to fracture in air at room temperature [42] (Fig. 13(c)).

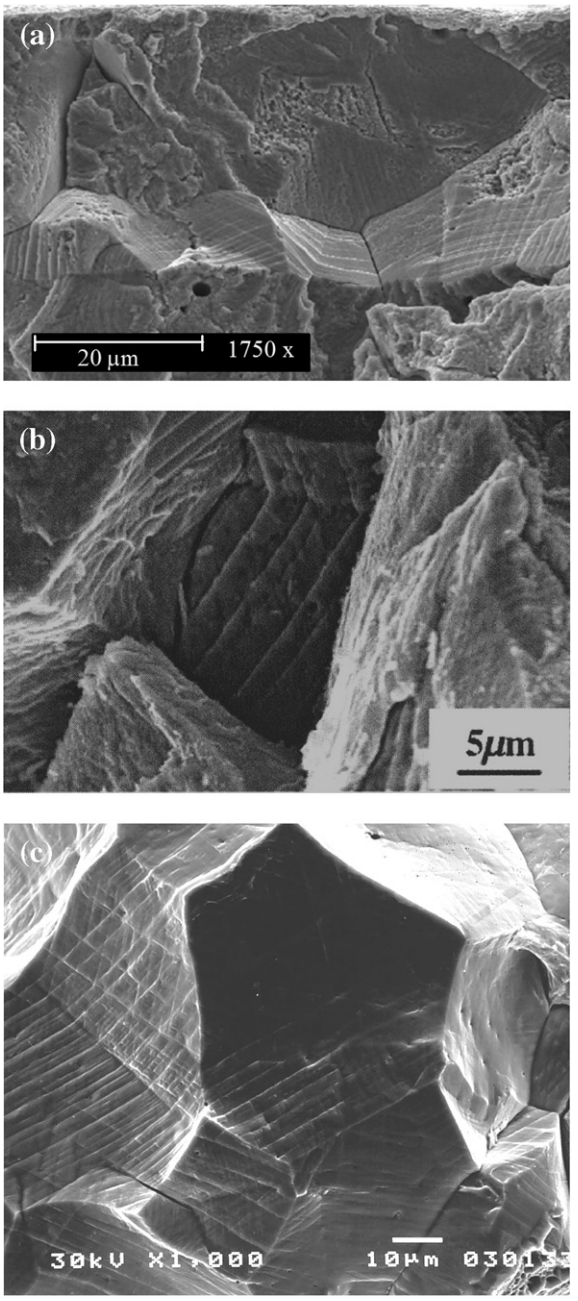

Fig. 13. SEM micrographs of the fracture surface of (a) proton-irradiated 304SS strained in BWR environment (from [40]), (b) thermally sensitized 304 SS neutron-irradiated to 1.2×10^{21} n/cm^2 ($E > 1$ MeV) in BWR condition and fractured in inert gas at 290 °C (from [41]), and (c) 304 SS neutron-irradiated to 30 dpa at 300 °C and strained to fracture in air at room temperature (from [42]). Steps on grain boundary facets are clearly visible in each micrograph.

5. Summary and conclusions

The objective of this work was to investigate the effect of localized deformation in A-286 precipitation-strengthened austenitic stainless steel on the SCC susceptibility in simulated primary water. The successive steps used and the main conclusions of this work are the following:

- A specific ageing heat treatment of 50 h at 670 °C defined in a previous study by the same authors was used. This ageing heat treatment leads to γ' mean diameter, volume fraction and density of 4.6 nm, 0.8% and 1.6×10^{23} m^{-3} respectively and does not lead to grain boundary η phase precipitation.
- Low cycle fatigue tests were first carried out on solution annealed (930 °C for 1 h) and aged A-286 specimens at 0.2% plastic strain control at $R = -1$ and 25 °C. Solution annealed A-286 work-harden for the first 50 cycles and then reach a plateau regime with no further evolution of the flow stress up to 1000 cycles. Aged A-286 work-harden for the first 20 cycles and then exhibit significant softening up to 1000 cycles.
- Cycling softening of aged A-286 is correlated with the formation of localized deformation bands due to shearing of γ' precipitates. γ' precipitates are believed to be completely dissolved after 120 fatigue cycles within the localized deformation bands. Average γ' precipitate-free localized deformation bands width and spacing of respectively 30 nm and 550 nm were statistically determined by TEM after 120 fatigue cycles.
- Comparative SCC tests were then performed on companion specimens having the same yield stress but with a few fatigue cycles, i.e. specimens with no precipitate-free localized deformation bands, and with several fatigue cycles, i.e. specimens with precipitate-free localized deformation bands. Results demonstrate that localized deformation significantly promotes A-286 IGSCC in PWR primary water.
- The approach developed in this study is believed to closely simulate strain localization in irradiated austenitic stainless steels and to give new

insights into the role played by strain localization in IASCC.

Acknowledgements

Financial support was provided by CEA/DSOE-RB. The authors gratefully acknowledge C. Lettori for her help with low-cycle fatigue testing at ENSMSE, C. Esnouf from INSA Lyon for his guidance in TEM, researchers from CEA/SCCME for the use of their facility for CERT testing in simulated PWR primary water, and researchers from CEA/SRMP for FEG-SEM examinations after SCC testing.

References

[1] G.S. Was, P.L. Andresen, JOM (April) (1992) 8.
[2] P. Scott, J. Nucl. Mater. 211 (1994) 101.
[3] T. Shoji, S. Suzuki, K.S. Raja, J. Nucl. Mater. 258–263 (1998) 241.
[4] J.T. Busby, G.S. Was, E.A. Kenik, J. Nucl. Mater. 302 (2002) 20.
[5] K. Fukuya, M. Nakano, K. Fujii, M. Kodama, T. Torimaru, in: Proceedings of the 11th International Symposium on Environmental Degradation of Materials in Nuclear Power Systems – Water Reactors, Stevenson, WA, August 10–14, 2003 (ANS), p. 1153.
[6] J.V. Sharp, Philos. Mag. 16 (1967) 77.
[7] D.J. Edwards, B.N. Singh, J.B. Bilde-Sorensen, J. Nucl. Mater. 342 (2005) 164.
[8] B.L. Eyre, A.F. Bartlett, Philos. Mag. 12 (1965) 261.
[9] S.J. Zinkle, B.N. Singh, J. Nucl. Mater. 351 (2006) 269.
[10] B. Mastel, H.E. Kissinger, J.J. Laidler, T.K. Bierlein, J. Appl. Phys. 34 (1963) 3637.
[11] J.I. Cole, H. Tsai, T.R. Allen, T. Yoshitake, N. Akasaka, I. Yamagata, Y. Nakamura, J. Nucl. Mater. 351 (2006) 316.
[12] J.I. Cole, S.M. Bruemmer, J. Nucl. Mater. 225 (1995) 53.
[13] N. Hashimoto, S.J. Zinkle, A.F. Rowcliffe, J.P. Robertson, S. Jitsukawa, J. Nucl. Mater. 283–287 (2000) 528.
[14] C. Bailat, A. Almazouzi, N. Baluc, R. Schaublin, F. Groschel, M. Victoria, J. Nucl. Mater. 283–287 (2000) 446.
[15] Y. Dai, X. Jia, J.C. Chen, W.F. Sommer, M. Victorai, G.S. Bauer, J. Nucl. Mater. 296 (2001) 174.
[16] B.H. Sencer, S.A. Maloy, M.L. Hamilton, F.A. Garner, J. Nucl. Mater. 345 (2005) 136.
[17] T.S. Byun, N. Hashimoto, K. Farell, J. Nucl. Mater. 351 (2006) 303.
[18] Z. Jiao, J.T. Busby, R. Obata, G.S. Was, in: Proceedings of the 12th International Symposium on Environmental Degradation of Materials in Nuclear Power Systems – Water Reactors, Salt Lake City, Utah, August 14–18, 2005 (TMS), p. 379.
[19] M. Savoie, et al., J. Nucl. Mater., doi:10.1016/j.jnucmat.2006.10.003.
[20] U. Essmann, U. Gosele, H. Mughrabi, Philos. Mag. 44 (1981) 405.
[21] M. Risbet, PhD thesis, Université de Technologie de Compiègne, 2002.
[22] M. Wilhelm, Mater. Sci. Eng. 48 (1981) 91.
[23] C.A. Stubbington, Acta Metall. 12 (1964) 931.
[24] D. Steiner, R. Beddoe, V. Gerold, G. Kostorz, R. Schmelezer, Scripta Metall. 17 (1983) 733.
[25] J.B. Clark, A.J. McEvily, Acta Metall. 12 (1964) 1359.
[26] C. Calabrese, C. Laird, Mater. Sci. Eng. 13 (1974) 141.
[27] S.P. Bhat, C. Laird, Acta Metall. 27 (1979) 1873.
[28] J.K. Lee, C. Laird, Mater. Sci. Eng. 54 (1982) 53.
[29] R.E. Stoltz, A.G. Pineau, Mater. Sci. Eng. 34 (1978) 275.
[30] M. Sundararaman, W. Chen, V. Singh, R.P. Wahi, Acta Metall. Mater. 38 (10) (1990) 1813.
[31] M. Sundararaman, W. Chen, R.P. Wahi, A. Wiedenmann, W. Wagner, W. Petry, Acta Metall. Mater. 40 (5) (1992) 1023.
[32] J.T. Busby, G.S. Was, in: Proceedings of the 11th International Symposium on Environmental Degradation of Materials in Nuclear Power Systems – Water Reactors, Stevenson, WA, August 10–14, 2003 (ANS), p. 995.
[33] P.L. Andresen, M.M. Morra, W.R. Catlin, Corrosion 2004, Paper No. 04678, New Orleans, March 28–April 1, 2004 (NACE).
[34] G. Li, Y. Kaneshima, T. Shoji, in: Proceedings of the 9th International Symposium on Environmental Degradation of Materials in Nuclear Power Systems – Water Reactors, Newport Beach, California, August 1–5, 1999 (TMS), p. 1,115.
[35] K.S. Raja, T. Masuda, T. Shoji, Y. Lee, in: Proceedings of the 9th International Symposium on Environmental Degradation of Materials in Nuclear Power Systems – Water Reactors, Newport Beach, California, August 1–5, 1999 (TMS), p. 1,125.
[36] J. Nakano, Y. Miwa, T. Kohya, T. Tsukada, J. Nucl. Mater. 329–333 (2004) 643.
[37] S.M. Bruemmer, E.P. Simonen, P.M. Scott, P.L. Andresen, G.S. Was, J.L. Nelson, J. Nucl. Mater. 274 (1999) 299.
[38] C. Pokor, Y. Brechet, P. Dubuisson, J.P. Massoud, A. Barbu, J. Nucl. Mater. 326 (2004) 19.
[39] K. Farrell, T.S. Byun, N. Hashimoto, ORNL Report ORNL/TM-2003/63, 2003.
[40] J.T. Busby, PhD thesis, University of Michigan, 2001.
[41] T. Onchi, K. Dohi, N. Soneda, J.R. Cowan, R.J. Scowen, M.L. Castano, J. Nucl. Mater. 320 (2003) 194.
[42] A. Toivonen, U. Ehrnsten, W. Karlsen, P. Aaltonen, J.-P. Massoud, J.-M. Boursier, in: Proceedings of the 12th International Symposium on Environmental Degradation of Materials in Nuclear Power Systems – Water Reactors, Salt Lake City, Utah, August 14–18, 2005 (TMS), p. 327.